文章编号：1001－9014(2016)03－0257－06

DOI:10.11972/j.issn.1001－9014.2016.03.001

Partial differential equation-based object extraction from remote sensing imagery

LI Zhong-Bin, SHI Wen-Zhong*

(Department of Land Surveying and Geo-Informatics, The Hong Kong Polytechnic University, Hong Kong, China)

Abstract: Object extraction is an essential task in remote sensing and geographical sciences. Previous studies mainly focused on the accuracy of object extraction method while little attention has been paid to improving their computational efficiency. For this reason, a partial differential equation (PDE)-based framework for semi-automated extraction of multiple types of objects from remote sensing imagery was proposed. The mathematical relationships among the traditional PDE-based methods, i.e., level set method (LSM), nonlinear diffusion (NLD), and active contour (AC) were explored. It was found that both edge- and region-based PDEs are equally important for object extraction and they are generalized into a unified framework based on the derived relationships. For computational efficiency, the widely used curvature-based regularizing term is replaced by a scale space filtering. The effectiveness and efficiency of the proposed methods were corroborated by a range of promising experiments.

Key words: active contour, building extraction, level set method, object extraction, partial differential equation, nonlinear diffusion, road extraction

PACS: 07.05. Pj

基于偏微分方程的遥感图像目标提取

李仲玢, 史文中*

(香港理工大学 土地测量与地理资讯学系,香港 中国)

摘要:从遥感图像中提取感兴趣的目标是遥感和地学领域的一个重要任务.先前的研究主要集中于目标提取的精度,而很少关注目标提取的效率.因此,作者提出一个基于偏微分方程的框架来进行半自动多类目标提取.首先,作者对水平集方法,非线性扩散,以及活动轮廓之间的数学关系进行了深入的探究.从探究的结果作者发现基于边缘和基于区域的偏微分方程在目标提取中同等重要,因此作者把它们概括成一个统一的框架.接着,为了使计算更加高效,作者用尺度空间滤波替换传统的曲率归一项.最后,作者通过一系列实验证明了该方法的有效性.

关 键 词:活动轮廓;建筑物提取;水平集方法;目标提取;偏微分方程;非线性扩散;道路提取

中图分类号:TP751 **文献标识码**:A

Introduction

Man-made object extraction has always been an intensive research topic in the field of applied Earth observation[1]. It is one of the most commonly used data acquisition methods in remote sensing and geographical sciences[2]. For instance, it is beneficial to the timely update of GIS database[3] and the decision-making of the urban planning. Generally, man-made objects in high spatial resolution remote sensing images appear as homogeneous regions with similar spectral signatures. However, automatic detection of man-made objects is still a challenging task. That is mainly because the complex

Received date: 2015-05-06, **revised date**: 2015-10-16 **收稿日期**:2015-05-06, **修回日期**:2015-10-16

Foundation items:Supported in part by Ministry of Science and Technology of China (2012BAJ15B04), by Research Grants Council of Hong Kong (PolyU 15223015, PolyU 5249/12E), by National Natural Science Foundation of China (41331175), by Leading Talent Project of the National Administration of Surveying (K.SZ.XX.VTQA)

Biography:LI Zhong-Bin(1985-), man, Cangxi, Sichuan, Ph.D. Research interests include remote sensing, land use and land cover change, and machine learning.

* **Corresponding author**:E-mail:lswzshi@polyu.edu.hk

scenes (e.g., bare land, cropland, vegetation, and shorelines) often share common features (e.g., geometric shape, radiometric intensity, or texture) with the desired objects[4-5]. Thus, there is a tremendous need to develop more operational object extraction methods[6]. This study primarily focuses on man-made object (i.e., roads and buildings) extraction from optical images using partial differential equation (PDE)-based methods. The aim of this paper is to propose practical semi-automated methods that can reduce user's load considerably.

PDE-based methods[7-12] have been widely used for object extraction from remote sensing imagery. Previous methods are mainly adapted from the region-based Chan-Vese (CV) model[13]. Cao and Yang[7] incorporate the fractal error metric and textural information into CV model for man-made object extraction from aerial images. Similar idea can be found in Ref. [8]. In Ref. [9], a region-based level set method (LSM) adapted from CV model was used to extract roads, buildings, and airport runways from satellite images. Xu, *et al.*[10] integrated intensity and texture information into CV model to extract salient objects from satellite images. Kim and Shan[11] extracted building roofs from point cloud data using the multiphase CV model. Ardila, *et al.*[12] used the region-based active contour to extract urban trees for change analysis. By contrast, edge-based methods have received much less attention for object extraction over the past decades. Laptev, *et al.*[14] used scale space theory and an edge-based parametric snake for rural road network extraction from aerial images. More recently, an edge-based level set evolution has been used to extract building roofs from aerial images[16], in which the initial level curves are generated using a corner detector. However, it has difficulties in handling man-made objects that do not have corners.

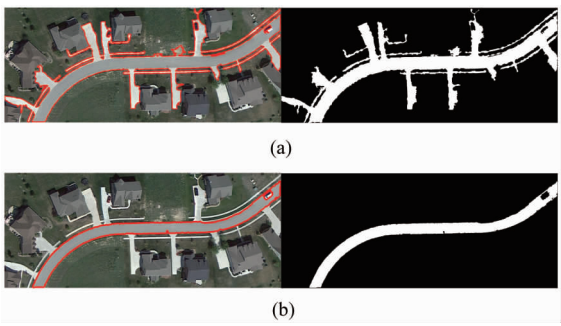

Fig. 1 Road extraction results obtained by PDE-based methods for road extraction. (a) Results of the model in Ref. [15] with $\lambda_1 = \lambda_2 = 1$. (b) Results of the proposed PDE-based method by Eq. (5) using data term defined in Eq. (8) with $\lambda_1 = -1$ and $\lambda_2 = -6$. Left: Original aerial images with extracted roads. Right: Corresponding binary results

图1 基于偏微分方程方法的道路提取结果. (a)模型[15]的结果,其中 $\lambda_1 = \lambda_2 = 1$. (b)本文提出的方法(公式(5))的结果,其中数据项由公式(8)表示,$\lambda_1 = -1$,$\lambda_1 = -6$. 左侧:原始航空图像和提取的道路. 右侧:对应的二值结果

Despite great efforts over the past years, it remains challenging to develop an operational approach for man-made object extraction from remote sensing imagery. Previous studies have been primarily focused on the accuracy of object extraction and little attention has been paid to improving the computational efficiency. In addition, some existing methods are very sensitive to parameter tuning. As shown in Fig. 1, different results are obtained using CV model with different parameter values. Thus, there is a need to develop new and practical methods for object extraction from remote sensing imagery.

This paper is outlined as follows. Section II describes the presented PDE-based framework in detail. Section III presents experimental results, including the qualitative and quantitative evaluations. Finally, the paper ends up with discussions and conclusions in Section IV.

1 Methodology

In this section, a brief review of the previous pioneering PDE-based methods, i.e., LSM[17], nonlinear diffusion (NLD)[18], and active contour (AC)[13, 19], is provided. Next, the mathematical relationships among these methods are explored in detail. Results indicate that both edge- and region-based PDEs are equally important for object extraction and they are thus generalized into a unified framework. For computational efficiency, the evolving zero-level sets are regularized by using a scale space filtering[20] instead of the traditionally used curvature term.

1.1 Previous work

1.1.1 Level set method

The basic idea behind LSM is to track and describe the evolution of the zero-level set in a higher dimensional level set function[17]. The original level set formulation is given as follows:

$$\phi_t = F(\kappa)\,|\nabla\phi| \quad , \quad (1)$$

where ϕ is the level set function. ϕ_t is the partial derivative of ϕ with respect to the temporal variable t. $\kappa = div(\nabla u/|\nabla u|)$ is the mean curvature of the zero-level set and $F(\kappa)$ is a function with respect to curvature κ. $F(\kappa)$ serves as not only the driving force in LSM (Eq. (1)), but also the regularization term to keep the moving zero-level set smooth.

1.1.2 Nonlinear diffusion

NLD proposed in Ref. [18] is given as follows:

$$u_t = g(|G_\sigma * \nabla u|)\,|\nabla u|\,div\left(\frac{\nabla u}{|\nabla u|}\right) \quad , (2)$$

where u_t is the partial derivative of u with respect to the time variable t; u is the image to be processed; $\nabla u = (u_x, u_y)$ is the gradient; $\nabla u = \sqrt{u_x^2 + u_y^y}$ is the magnitude of ∇u; G_σ is the Gaussian kernel with standard deviation σ; $*$ is the convolution operator; div is the divergence operator; $div(\nabla u/|\nabla u|)$ is the mean curvature as before; and $g(\cdot)$ is an edge detector with respect to the gradient such as $g(|\nabla u|) = 1/(1 + |\nabla u|^2)$. In low-level vision, NLD (Eq. (2)) was widely used for the noise removal. The term $|\nabla u|div(\nabla u/|\nabla u|)$ diffuses along the boundaries but not across them under the control of the stopping term $g(|G_\sigma * \nabla u|)$[21].

1.1.3 Edge-based active contour

The seminal parametric snakes was first proposed in

Ref. [22]. However, it has difficulty in handling topological changes naturally. In contrast, geometrical models perform much better such as the edge-based active contour (EAC) proposed in Ref. [19]:

$$\phi_t = g|\nabla\phi|\left[div\left(\frac{\nabla\phi}{|\nabla\phi|}\right)+V\right] \quad , \quad (3)$$

in which ϕ is the level set function as before. g is the same as the one in NLD. Compared with NLD, EAC (Eq. (3)) has one more positive real constant v, which can keep the term $div(\nabla\phi/|\nabla\phi|)+v$ always positive. It is clear that EAC (Eq. (3)) is essentially equivalent to NLD (Eq. (2)). The differences between them are twofold: 1) the former is originally developed for object extraction, whereas the latter is proposed for noise removal, and 2) the former often chooses signed distance function as level set function; whereas the latter often uses the original image as level set function.

1.1.4 Region-based active contour

In practical applications, EAC often suffers from limitations, e.g., 1) it is sensitive to noises and 2) it cannot extract the interior edges. To address these issues, region-based active contour (RAC) is proposed[13]:

$$\phi_t = \delta_\varepsilon(\phi)\left[\mu div\left(\frac{\nabla\phi}{|\nabla\phi|}\right)-v-\lambda_1(I_0-c_1)^2+\lambda_2(I_0-c_2)^2\right] \quad , \quad (4)$$

in which $\delta_\varepsilon(\cdot)$ is the Dirac function; $\mu\geqslant 0, v\geqslant 0$, and $\lambda_1,\lambda_2>0$ are free parameters; I_0 is the original image; and c_1, c_2 are intensity means inside and outside the zero-level set, respectively. Although RAC (Eq. (4)) is more advantageous than EAC, it also suffers from limitations. For instance, there are too many parameters in Eq. (4) that need to be tuned repeatedly before it can be employed in practical applications. However, it is often labor-intensive and time-consuming to obtain the optimal parameter values.

1.2 The proposed method

Based on the above analysis, some unexpected mathematical relationships among LSM[17], NLD[18], EAC[19], and RAC[13] can be derived as follows:

1) NLD and EAC are theoretically equivalent when the level set function in Eq. (3) equals the image in Eq. (2), i.e., $\phi = u$.

2) PDE-based methods (i.e., NLD, EAC, and RAC) can be viewed as further developments of LSM, though they are derived from different mathematical models. In contrast to LSM, NLD and EAC take advantage of the edge detector $g(\cdot)$ as stopping term, whereas RAC employs intensity means as the stopping term.

3) As can be seen, when $g(|G_\sigma * \nabla u|)=1$, Eq. (2) becomes Eq. (1). When $g=1$ and $v=0$, Eq. (3) becomes Eq. (1). In addition, Eq. (4) becomes Eq. (1) when $\delta_\varepsilon(\phi)=|\nabla\phi|$, $\mu=1$, $\lambda_1=\lambda_2=v=0$.

4) All the aforementioned PDE-based methods can be implemented using finite difference scheme.

The unexpected relationships mentioned above make it easier to understand the essences of PDE-based methods. It is worth mentioning that the Dirac function δ_ε in Eq. (4) can be replaced by $|\nabla\phi|$[13]. In addition, according to the theory in Ref. [23], it is mathematically sound to replace the curvature term $div(\nabla\phi/|\nabla\phi|)$ commonly used in traditional PDE-based methods by the scale space filtering. It has been proved that the best filtering for constructing scale space is the Gaussian kernel G_σ[24]. Based on all these facts, it can be found that both edge- and region-based PDE-based approaches are equally important in practical applications, and thus, they are generalized into the following unified framework:

$$\phi_{i,j}^{n+1} = G_\sigma * sign(\phi_{i,j}^n + \Delta t * F|\nabla\phi_{i,j}^n|) \quad , (5)$$

where (i,j) denotes spatial position; n means iteration number; $sign(\cdot)$ is the sign function; Δt is the time step; and F is the data term that is used to guide active contours toward desired object boundaries. In Eq. (5), $\phi_{i,j}^n$ is defined as follows:

$$\phi_{i,j}^0 = \begin{cases} c_0, & \text{if } (i,j)\in R_0 \\ -c_0, & \text{otherwise} \end{cases} \quad , \quad (6)$$

in which $c_0>0$ is a constant. It is fixed at 1 in this study. R_0 is an arbitrarily given region (i.e., the initial zero-level set) in the image domain. Essentially, PDE (Eq. (5)) can be regarded as a further development of the seminal LSM, which is the most basic component of the popular methods NLD, EAC, and RAC. F in Eq. (1) is a function with regard to the curvature of zero-level set, whereas F in Eq. (5) is a generic data term that can be specifically written as follows:

$$F_E = g(G_\sigma * |\nabla I|) \quad , \quad (7)$$

$$F_R = -\lambda_1(I-c_1)^2+\lambda_2(I-c_2)^2 \quad , \quad (8)$$

where F_E and F_R are edge- and region-based data terms, respectively. I is the image to be processed. In fact, data terms defined by Eqs. (7) and (8) are derived from EAC and RAC, respectively. Despite this, it leads to a considerable improvement of the original LSM. That is corroborated by the following experiments.

1.3 The implementation of the proposed method

PDE is an iterative process that exploits finite difference scheme to approximate its solution. Before its implementation, initial zero-level sets need to be given in the desired object regions interactively. In this paper, for numerical stability, scale space technique is used to regularize the evolving zero-level sets. The basic idea of this technique is to convolve the level set function with a scale space filtering from coarser to finer scales[23]. With the increase of the scale parameter σ, the level set function becomes coarser and smoother, and noises disappear in coarser scales. In this respect, it is very useful for edge-based PDE-based methods such as NLD and EAC as they are often sensitive to noise.

However, different from PDE methods NLD and EAC, in which the scale space filtering is mainly used for noise removal, PDE Eq. (5) mainly utilizes scale space filtering to convolve the iterated level set function, thus 1) removing small spurious objects and 2) making the level set function regular during evolution.

Overall, the advantages of the proposed PDE-based method over other existing methods in the following three aspects:

1) LSM does not take into account data term. This means that it cannot be used for object extraction directly. In contrast, the proposed PDE Eq. (5) takes advantage of the image features (e.g., the edge detector in Eq. (7) and the intensity mean in Eq. (8) to drive the

zero-level set toward desired object boundaries.

2) To maintain the moving zero-level set smooth, the traditional approaches represented by Eqs. (1-4) exploit the curvature of the zero-level set; the proposed method (Eq. (5)), in contrast, uses the scale space filtering to convolve the zero-level set directly.

3) For numerical stability, traditionally methods can only use a very small time step, and thus, they often consume too much CPU time. By contrast, the proposed method can use a relatively larger time step due to the removal of the curvature. In this respect, it is computationally much more efficient.

In the next section, a range of experiments is demonstrated to verify the effectiveness of the proposed method.

2 Experiments

2.1 Dataset and experiment setup

In this experiment, six remote sensing images acquired from different sensors were used to test the proposed methods. As shown in Figs. 2 and 3, they are named R_1, R_2, B_1, B_2, S_1, and S_2 (R, B, and S denote road, building, and stadium), respectively. They all contain three bands (i.e., R, G, and B), except for R_2 that just has the panchromatic band. As shown in the figures, road networks in R_1 and R_2 have opposite intensities. Building in B_1 is very noisy. Stadiums in S_1 and S_2 have different illuminations and there are intensity variations inside the stadium in R_2. In addition, as all the desired objects are characterized by different shapes, they can be used to validate the capability of the proposed method to extract objects without the need of the geometrical a priori information. The detailed information of these images is given in Table I. To corroborate the advantages of the proposed method, it was compared with EAC and RAC in all the experiments. All the experimental results were compared with ground truths qualitatively and quantitatively. Ground truths are generated by manual delineation. For quantitative evaluation, three indices are used[16], i.e., *Completeness* = TP_M/TP_{gt}, *Completeness* = TP_M/TP_e, and *Completeness* = TP_M/TP_{umgt}, in which TP_M is the total pixel number of the extracted object that is matched with the ground truth, TP_{gt} is the total pixel number of the ground truth, TP_e is the total pixel number of the extracted object, and TP_{umgt} is the total pixel number of the ground truth that is unmatched with the extracted object. The proposed algorithms were run under MATLAB R2013a 64 b in Windows 7 OS with Intel(R) Core(TM) i7-3770 CPU @ 3.40 GHz, 16 GB RAM. The source code will be publicly available at http://www.lsgi.polyu.edu.hk/academic_staff/John.Shi/index.htm.

Table 1 Dataset description (SR means spatial resolution)
表1 数据集描述(SR表示空间分辨率)

Images (SR: meter)	Sensor	Size (pixel × pixel)	Location
R_1 (0.1)	Aerial	1722 × 2321	Indiana, USA
R_2 (0.5)	Worldview-1	267 × 439	N/A
B_1 (0.5)	Pleiades-1	291 × 265	Washington, USA
B_2 (0.5)	Pleiades-1	329 × 334	Melbourne, Australia
S_1 (0.5)	Pleiades-1	532 × 519	Fortaleza, Brazil
S_2 (0.5)	Pleiades-1	463 × 529	Salvador, Brazil

Table 2 Parameter values used in each test methods
表2 每个测试方法所用的参数值

Images	EAC (3)	RAC (4)	PDE (7)	PDE (8)
R_1	$\Delta t=0.2, v=3$	$\mu=\Delta t=0.5, v=5\,000, \lambda_1=-1, \lambda_2=-4.5$	$\sigma_1=1, \sigma_2=1$	$\sigma=1, \lambda_1=-1, \lambda_2=-6$
R_2	$\Delta t=0.2, v=3$	$\mu=\Delta t=0.5, v=0, \lambda_1=-1, \lambda_2=1$	$\sigma_1=1, \sigma_2=1$	$\sigma=1, \lambda_1=\lambda_2=1$
B_1	$\Delta t=0.2, v=3$	$\mu=\Delta t=0.5, v=0, \lambda_1=-1, \lambda_2=1$	$\sigma_1=1.5, \sigma_2=1.5$	$\sigma=1.5, \lambda_1=\lambda_2=1$
B_2	$\Delta t=0.2, v=3$	$\mu=\Delta t=0.5, v=0, \lambda_1=1, \lambda_2=1$	$\sigma_1=1.5, \sigma_2=1.5$	$\sigma=1.5, \lambda_1=\lambda_2=1$
S_1	$\Delta t=0.2, v=3$	$\mu=\Delta t=0.5, v=0, \lambda_1=1, \lambda_2=1$	$\sigma_1=1.5, \sigma_2=1.5$	$\sigma=1.5, \lambda_1=\lambda_2=1$
S_2	$\Delta t=0.2, v=3$	$\mu=\Delta t=0.5, v=0, \lambda_1=1, \lambda_2=1$	$\sigma_1=1.5, \sigma_2=1.5$	$\sigma=1.5, \lambda_1=\lambda_2=1$

2.2 Parameter tuning

All the parameters used in the test methods are listed in Table 2. The parameter values in EAC and RAC are determined via trial and error. The free parameters λ_1 and λ_2 in RAC have significant impacts on final results. Sometimes they are not equal to each other such as in the experiment of R_1 (see Fig. 1). Throughout the experiments, the template size of the Gaussian kernel is fixed as 9×9. Generally, the use of a relatively larger time step Δt can expedite the iteration of PDE-based methods. However, it may lead to unstable numerical results. To obtain stable results using traditional methods such as NLD, EAC, and RAC, the time step should be sufficiently small due to the curvature term $div(\nabla u/|\nabla u|)$ or $div(\nabla\phi/|\nabla\phi|)$. Thus, a relatively small time step is often utilized. By contrast, due to the removal of the curvature term in the proposed PDE, the time step can be chosen as up to 40 for both the edge- and region-based PDEs (Eqs. (7) and (8)). Nevertheless, it is fixed at 18 for stable results in all the experiments. In addition, it is worth noting that edge-based model defined with Eq. (7) use the Gaussian kernel twice: once for the noise removal of the original image and once for the regularization of the zero-level set. Thus, there are two scale parameters σ_1 and σ_2 need to be tuned for Eq. (7). However, experiments show that the optimal pa-

Table 3 Quantitative results of the test methods
表3 测试方法的定量评价结果

Indices	Completeness(%)						Correctness(%)						Quality(%)					
Images	R_1	R_2	B_1	B_2	S_1	S_2	R_1	R_2	B_1	B_2	S_1	S_2	R_1	R_2	B_1	B_2	S_1	S_2
EAC (3)	96.4	79.3	78.0	92.0	97.7	32.7	86.9	87.7	89.6	97.7	98.6	98.5	75.8	64.9	66.1	88.1	95.1	32.4
RAC (4)	97.3	93.6	86.3	97.6	97.0	99.7	75.4	90.9	92.8	95.0	99.5	98.8	60.3	77.9	75.9	88.5	96.1	97.3
PDE (7)	97.4	71.0	73.4	76.8	87.0	96.0	98.4	97.7	99.9	99.9	100	100	94.5	68.6	73.3	76.8	87.0	96.0
PDE (8)	97.6	92.8	89.0	93.5	95.6	99.0	94.0	88.0	91.3	91.0	99.0	98.7	86.7	74.1	76.1	78.9	93.8	96.4

rameter values are readily available.

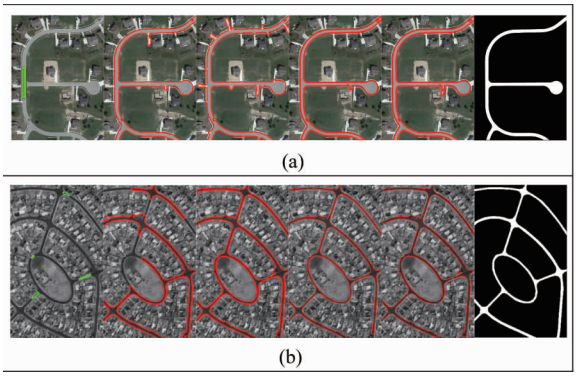

Fig. 2　Results for road extraction with different methods. (a) Aerial image R_1 with the bright road. (b) Satellite image R_2 with the dark road. From left to right: original images with green initial zero-level sets, results of EAC (3), RAC (4), edge--based and region-based PDE, and the ground truths, respectively

图 2　所有测试方法的道路提取结果. (a)航空图像 R_1 和明亮道路. (b)卫星图像 R_2 和暗色道路. 从左到右:原始图像和绿色的初始零水平集,EAC(3)的结果,RAC(4)的结果,PDE(7)的结果,PDE(8)的结果,和参考值

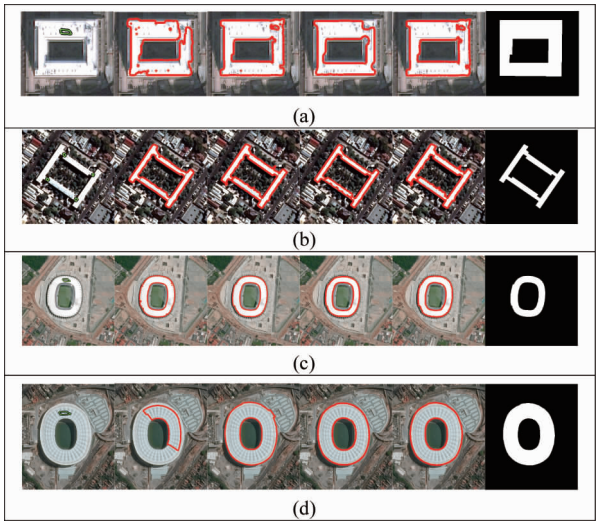

Fig. 3　Results of the test methods for building extraction from satellite images. (a) Building B_1 with heavy noises. (b) Building B_2 with complicated backgrounds. (c) Bright homogeneous stadium S_1. (d) Dark heterogeneous stadium S_2. From left to right: original images with green initial zero-level sets, results of EAC (3), RAC (4), edge--based and region-based PDE, and the ground truths, respectively

图 3　所有测试方法的建筑物提取结果. (a)有噪声的建筑物 B_1. (b)有复杂背景的建筑物 B_2. (c)明亮匀质的体育馆 S_1. (d)暗色异质的体育馆 S_2. 从左到右:原始图像和绿色的初始零水平集,EAC(3)的结果,RAC(4)的结果,PDE(7)的结果,PDE(8)的结果,和参考值

2.3　Qualitative evaluation

As presented in Figs. 2-3, the proposed PDEs are capable of extracting multiple types of man-made objects from optical images. All the initial zero-level sets in the experiments are manually provided inside the object regions.

Figure 2 shows how the proposed methods can extract bright and dark roads from images R_1 and R_2, respectively. Despite the over-detection in some areas, they can extract the road networks completely. Different from the model in Ref. [15], which extracts the neighboring sideways (see Fig. 1), the proposed methods can extract the desired road networks accurately. As can be seen, over-detection occurs in the results of EAC and RAC in R_1. In addition, EAC cannot obtain the complete dark road network in R_2.

Figure 3 shows how they can extract the buildings and stadiums without the need of a priori geometric information. As shown in the figures, the proposed methods are capable of extracting the rectangular building with heavy noises from image B_1, and noises are automatically filtered out by the scale-space filtering, as presented in Fig. 3(a). The specific scale parameters σ_1, and σ_2 are given in Table 2. Also, they successfully extract the building immersed in the complex backgrounds from image B_2, examining Fig. 3(b). In addition, they are able to extract the elliptic stadiums from images S_1 and S_2 accurately, as presented in Fig. 3(c) and (d). The stadium in S_1 is bright and homogeneous, whereas the one in S_2 is relatively dark and heterogeneous. Despite this, the proposed PDEs can extract them accurately. By contrast, EAC performs relatively poor. It cannot extract the building in B_1 completely, and it only extracts part of the stadium in S_2 due to the heavy intensity variations.

Table 4　Running times of the test methods (unit: second)
表 4　测试方法的运行时间(单位:秒)

Images	R_1	R_2	B_1	B_2	S_1	S_2
EAC (3)	7991.6	98.8	80.0	23.0	375.5	517.2
RAC (4)	3596.5	25.7	10.3	4.1	52.4	46.5
PDE (7)	230.5	0.7	0.7	0.3	2.2	3.5
PDE (8)	293.1	1.0	0.6	0.3	3.1	2.7

2.4　Quantitative evaluation

The quantitative evaluation results of the proposed PDEs for man-made object extraction are given in Table III. Overall, they have comparable quality to the traditional methods (i.e., EAC and RAC) in all the experiments. In comparison with the edge-based methods (i.e. EAC and PDE (7)), region-based methods (i.e., RAC and PDE (8)) have better *completeness*. That is mainly because the original images need to be smoothed by scale space filtering in edge-based methods, and thus, edges become blurred and their locations are shifted in some sense. However, this denoising step is unnecessary in region-based methods. Sometimes the *correctness* of region-based methods is not as great as edge-based methods, as indicated by the bold text in Table 3. That is because region-based methods often detect neighboring undesired objects that are spectrally similar to the desired ones. From the perspective of *quality*, the performance of the proposed edge-based PDE method is not as great as other methods in B_2 and S_1. However, it outperforms EAC in other experiments. In addition, the proposed region-based PDE method clearly excels RAC

in experiments of R_1. However, they have similar performance in other experiments. In terms of running time, the proposed methods outperform EAC and RAC significantly, as shown in Table 4. In all the experiments, the proposed edge-based method is 35, 141, 114, 77, 171, and 148 times faster than EAC; the proposed region-based method is 12, 26, 17, 14, 17, and 17 times faster than RAC. Thus, the proposed methods are computationally much more efficient than the traditional methods.

3 Discussion and conclusion

This paper has presented a PDE-based unified framework for object extraction from remote sensing imagery. Essentially, the framework is derived from the unexpected relationships among the traditional level set method (LSM), nonlinear diffusion (NLD), and active contour (AC). The curvature term widely used in traditional PDE-based methods is replaced by the scale space filtering in the new framework, which makes it possible to use a larger time step in the numerical scheme. Meanwhile, this scale space filtering can keep the moving zero-level sets regular while filtering out noises. The proposed framework is finally implemented by using finite difference scheme. Experiments indicate that it is computationally much more efficient than previous methods while obtaining comparable performance.

In future research, it would be necessary to automate the proposed PDE-based methods. Also, it would be interesting to improve traditional PDE-based methods such as NLD and LSM by taking advantage of texture and spatial contexture information. Finally, the attention can be paid to extracting natural objects such as tree crown, cropland, and forest from remote sensing imagery.

Acknowledgment

The authors would like to thank Prof. Cem Unsalan, Yeditepe University for providing the GeoEye-1 panchromatic image R_2. Also, they would like to thank the handling editor and the two anonymous reviewers for their valuable and detailed comments, which improved the quality of the manuscript substantially.

References

[1] Trinder J C. Workshop on automatic extraction of man-made objects from aerial and space images [J]. *ISPRS Journal of Photogrammetry and Remote Sensing*, 1995, **50**: 33 - 34.

[2] Heipke C, Pakzad L, Straub B M. Image analysis for GIS data acquisition [J]. *Photogrammetry Record*, 2000, **16**: 963 - 983.

[3] Jodouin S, Bentabet L, Ziou D, *et al*. Spatial database updating using active contours for multispectral images: application with Landsat 7 [J]. *ISPRS Journal of Photogrammetry and Remote Sensing*, 2003, **57**: 346 - 355.

[4] Baltsavias E P. Object extraction and revision by image analysis using existing geodata and knowledge: current status and steps towards operational systems [J]. *ISPRS Journal of Photogrammetry and Remote Sensing*, 2004, **58**: 129 - 151.

[5] DellAcqua F, Gamba P, Lisini G. Rapid mapping of high resolution SAR scenes [J]. *ISPRS Journal of Photogrammetry and Remote Sensing*, 2009, **64**: 482 - 489.

[6] Mayer H. Object extraction in photogrammetric computer vision [J]. *ISPRS Journal of Photogrammetry and Remote Sensing*, 2008, **63**: 213 - 222.

[7] Cao G and Yang X. Man-made object detection in aerial images using multi-stage level set evolution [J]. *International Journal of Remote Sensing*, 2007, **28**: 1747 - 1757.

[8] Wei W, Xin Y. Feature extraction for man-made objects segmentation in aerial images [J]. *Machine Vision and Applications*, 2008, **19**: 57 - 64.

[9] Karantzalos K, Argialas D. A region-based level set segmentation for automatic detection of man-made objects from aerial and satellite images [J]. *Photogrammetric Engineering and Remote Sensing*, 2009, **75**: 667 - 677.

[10] Xu Q Z, Li B, He Z F, *et al*. Multiscale contour extraction using a level set method in optical satellite images [J], *IEEE Geoscience and Remote Sensing Letters*, 2011, **8**: 854 - 858.

[11] Kim K, Shan J. Building roof modeling from airborne laser scanning data based on level set approach [J]. *ISPRS Journal of Photogrammetry and Remote Sensing*, 2011, **66**: 484 - 497.

[12] Ardila J P, Biker W, Tolpekin A, *et al*. Multitemporal change detection of urban trees using localized region-based active contours in VHR images [J]. *Remote Sensing of Environment*, 2012, **124**: 413 - 426.

[13] Chan T F, Vese L A. Active contours without edges [J]. *IEEE Transactions on Image Processing*, 2001, **10**: 266 - 277.

[14] Laptev I, Mayer H, Lindeberg T, *et al*. Automatic extraction of roads from aerial images based on scale space and snakes [J]. *Machine Vision and Applications*, 2000, **12**: 23 - 31.

[15] Zhang K H, Zhang L, Song H H, *et al*. Active contours with selective local or global segmentation: a new formulation and level set method [J]. *Image and Vision Computing*, 2010, **28**: 668 - 676.

[16] Cote M, Saeedi P. Automatic rooftop extraction in Nadir aerial imagery of suburban regions using corners and variational level set evolution [J]. *IEEE Transactions on Geoscience and Remote Sensing*, 2013, **51**: 313 - 328.

[17] Osher S, Sethian J A. Fronts propagating with curvature-dependent speed - algorithms based on Hamiltion-Jacobi formulations [J]. *Journal of Computational Physics*, 1988, **79**: 12 - 49.

[18] Alvarez L, Lions P L, Morel J M. Image selective smoothing and edge-detection by nonlinear diffusion [J]. *SIAM Journal of Numerical Analysis*, 1992, **29**: 845 - 866.

[19] Caselles V, Catte F, Coll T, *et al*. A geometrical model for active contours in image processing [J]. *Numerische Mathematik*, 1993, **66**: 1 - 31.

[20] Witkin A P. Scale-space filtering: A new approach to multi-scale description [C]. *IEEE International Conference on Acoustics, Speech, and Signal Processing*, 1984, 150 - 153.

[21] Carmona R A, Zhong S F. Adaptive smoothing respecting feature directions [J]. *IEEE Transactions on Image Processing*, 1998, **7**: 353 - 358.

[22] Kass M, Witkin A, Terzopoulos D. Snakes - active contour models [J]. *International Journal of Computer Vision*, 1987, **1**: 321 - 331.

[23] Perona P, Malik J. Scale-space and edge-detection using anisotropic diffusion [J], *IEEE Transactions on Pattern Analysis and Machine Intelligence*, 1990, **12**: 629 - 639.

[24] Babaud J, Witkin A, Baudin M, *et al*. Uniqueness of the Gaussian kernel for scale-space filtering [J], *IEEE Transactions on Pattern Analysis and Machine Intelligence*, 1986, **8**: 26 - 33.